Spin Relaxation in Single-Layer and Bilayer Graphene

Wei Han and R. K. Kawakami

Phys. Rev. Lett. **107**, 047207 — Published 21 July 2011

DOI: 10.1103/PhysRevLett.107.047207

`

Spin Relaxation in Single Layer and Bilayer Graphene

Wei Han and R. K. Kawakami[†]

Department of Physics and Astronomy, University of California, Riverside, CA 92521

[†] e-mail: roland.kawakami@ucr.edu

Abstract:

We investigate spin relaxation in graphene spin valves and observe strongly contrasting behavior for single layer graphene (SLG) and bilayer graphene (BLG). In SLG, the spin lifetime (τ_s) varies linearly with the momentum scattering time (τ_p) as carrier concentration is varied, indicating the dominance of Elliot-Yafet (EY) spin relaxation at low temperatures. In BLG, τ_s and τ_p exhibit an inverse dependence, which indicates the dominance of Dyakonov-Perel spin relaxation at low temperatures. The different behavior is due to enhanced screening and/or reduced surface sensitivity of BLG, which greatly reduces the impurity-induced EY spin relaxation.

PACS numbers: 85.75.-d, 81.05.ue, 72.25.Rb, 72.25.Hg

`

Graphene is an attractive material for spintronics due to the possibility of long spin lifetimes arising from low intrinsic spin-orbit coupling and weak hyperfine coupling [1-5]. However, Hanle spin precession experiments in graphene spin valves report spin lifetimes that are orders of magnitude shorter than expected theoretically [6-12]. This has prompted theoretical studies of the extrinsic sources of spin relaxation such as impurity scattering [13], ripples [5], and substrate effects [14]. Experimentally, several studies have investigated spin relaxation including the roles of impurity scattering [7, 11] and graphene thickness [15]. Recently, it has been shown that ferromagnet (FM) contact-induced spin relaxation is responsible for the short spin lifetimes observed in experiments [12]. Therefore, high quality tunneling contacts are necessary to suppress the contact-induced effects for systematic investigations of spin relaxation in graphene.

In this Letter, we perform systematic studies of spin relaxation in single layer graphene (SLG) and bilayer graphene (BLG) spin valves with tunneling contacts. The dependence of spin lifetime on temperature and carrier concentration (tuned by gate voltage) reveals rather different spin relaxation mechanisms in the two systems. In SLG, the temperature dependence shows similar trends of the spin lifetime and momentum scattering time, and the low temperature gate voltage dependence shows a strong linear scaling of the two quantities. This indicates the dominance of Elliot-Yafet (EY) spin relaxation, which most likely comes from impurity scattering. In BLG, the temperature dependence and low temperature gate voltage dependence show a nearly inverse relationship between the spin lifetime and momentum scattering time. This indicates the dominance of Dyakonov-Perel (DP) spin relaxation, which can be generated by ripples in the graphene. The contrasting behaviors of SLG and BLG can be understood as a reduction of the impurity scattering in BLG due to the enhanced screening of the impurity potential and reduced surface sensitivity. This leads to longer spin lifetimes (~6.2 ns, the highest

`

value observed in graphene spin valves to date) and the greater role of DP spin relaxation observed in BLG.

The graphene flakes are mechanically exfoliated from HOPG onto an SiO_2 (300 nm thickness)/Si substrate [16]. Gate voltage is applied to the Si substrate to tune the carrier concentration in graphene. SLG and BLG are identified by optical microscopy and Raman spectroscopy [17]. Standard e-beam lithography with PMMA/MMA bilayer resist is used to define the Au and Co electrodes. First, two Au electrodes are put down on the two ends of the graphene. Then a second step of e-beam lithography is used for the Co electrodes, where subsequent angle evaporations of TiO_2, MgO, and Co produce the ferromagnetic electrodes with tunneling contacts [12, 18]. Typically several Co electrodes are fabricated in between the two Au electrodes, but only two Co electrodes are wired up for the nonlocal measurement.

Studies of spin transport and spin relaxation are performed on graphene spin valves consisting of two spin-sensitive Co electrodes (E2, E3) and two Au electrodes (E1, E4). Nonlocal voltages (V_{NL}) are measured using lock-in detection with an ac injection current of I = 1 μA rms at 13 Hz [18]. The nonlocal resistance ($R_{NL} = V_{NL}/I$) is measured as a function of in-plane magnetic field (Fig. 1a inset) to detect the spin injection and transport [6, 19-24]. Figures 1a show the nonlocal magnetoresistance (MR) curves for a typical SLG device (Device A), in which the sharp changes in R_{NL} are due to the magnetization switching of the Co electrodes. The nonlocal MR (ΔR_{NL}) is indicated by the red arrow, which is the magnitude of the sharp change in R_{NL}.

The spin lifetime (τ_s), diffusion coefficient (D), and spin diffusion length ($\lambda = \sqrt{D\tau_s}$) are determined by the Hanle spin precession measurement (figure 1b inset) [20]. Applying an out-of-plane magnetic field ($H_\perp$) causes the spins to precess as they diffuse from E2 to E3, which

`

results in characteristic Hanle curves as shown for devices A at 300 K (figure 1b). The red circles (black circles) are for the parallel (antiparallel) alignment of the Co magnetizations. τ_s and D are determined by fitting the Hanle curves with

$$R_{NL} \propto \pm \int_0^\infty \frac{1}{\sqrt{4\pi Dt}} \exp[-\frac{L^2}{4Dt}] \cos(\omega_L t) \exp(-t/\tau_s) dt \quad (1)$$

where the + (-) sign is for the parallel (antiparallel) magnetization state, L is the spacing between the Co electrodes, $\omega_L = g\mu_B H_\perp / \hbar$ is the Larmor frequency, g is the g-factor, μ_B is the Bohr magneton, and $\hbar$ is the reduced Planck's constant. For device A, D = 0.013 m^2/s, τ_s = 447 ps, and λ_G = 2.4 μm. The τ_s and D obtained from the Hanle curves are plotted as a function of gate voltage in Figure 1c and 1d for 300K and 4K respectively. At 300 K, there is no obvious correlation between τ_s and D. Interestingly, when the device is cooled to T = 4 K, τ_s and D exhibit a strong correlation, with both quantities increasing with carrier concentration. The correlation of τ_s and D implies a linear relation between τ_s and the momentum scattering time, τ_p ($D \sim \tau_p$ as discussed in refs. [7, 15, 25]). This indicates that at low temperatures the spin scattering is dominated by momentum scattering through the EY mechanism (i.e. finite probability of a spin-flip during a momentum scattering event) [26-28]. This behavior has been observed in five SLG devices (mobility: 1000-3000 cm^2/Vs).

The temperature dependences of τ_s and D at different carrier concentrations are shown in Figures 2a and 2b. As the temperature decreases from 300 K to 4 K, τ_s shows a modest increase at higher carrier densities (e.g. from ~0.5 ns to ~1 ns for $V_g - V_{CNP}$ = +60 V) and little variation for lower carrier densities. The temperature dependence of D shows a similar behavior as τ_s. To analyze the relationship between the spin scattering and momentum scattering, we plot τ_s vs. D

`

for temperatures T = 4 K (figure 2c), T = 10 K (figure 2d), T = 50 K and 100 K (figure 2e), T = 200 K and 300 K (figure 2f), respectively. The main trend is that for lower temperatures, τ_s scales linearly with D, which indicates that an EY spin relaxation mechanism is dominant at lower temperatures (≤100 K). For higher temperatures, τ_s and D do not follow the linear relationship as shown at low temperatures, which suggests that multiple sources of spin scattering are present. If there is more than one source of EY spin scattering (e.g. impurities of different species, phonons, etc.), the linear relationship between τ_s and τ_p does not necessarily hold; for example, with two EY scattering mechanisms obeying $\tau_{s,1}^{-1} = k_1 \tau_{p,1}^{-1}$ and $\tau_{s,2}^{-1} = k_2 \tau_{p,2}^{-1}$, the overall spin relaxation rate $\tau_s^{-1} = \tau_{s.1}^{-1} + \tau_{s,2}^{-1} = k_1\left(\tau_{p,1}^{-1} + \frac{k_2}{k_1}\tau_{p,2}^{-1}\right)$ is not proportional to the overall momentum scattering rate $\tau_p^{-1} = \tau_{p,1}^{-1} + \tau_{p,2}^{-1}$ except in some special cases (e.g. $k_1 = k_2$, $\tau_{p,1} \ll \tau_{p,1}$, etc.).

Next, we investigate spin relaxation in BLG spin valves, which differs from SLG not just in thickness but also in band structure (linear for SLG, parabolic for BLG) and intrinsic spin-orbit coupling [29, 30]. Figure 3a shows the Hanle curve of the longest observed spin lifetime of 6.2 ns, which is obtained on device B for the charge neutrality point at 20 K. Figure 3a inset shows the Hanle curve at 300 K with best fit parameters of τ_s = 268 ps. The gate voltage dependences of τ_s and D at 300 K and 20 K are shown in Figure 3b and 3c, respectively. At 300 K, τ_s varies from 250 ps to 450 ps as a function of gate voltage and exhibits no obvious correlation with D. At 20 K, τ_s varies from 2.5 ns to 6.2 ns, showing a peak at the charge neutrality point. On the other hand, the gate voltage dependence of D exhibits lower values near the charge neutrality point and increasing values at higher carrier densities. The opposite behaviors of τ_s and D

`

suggest the importance of DP spin relaxation (i.e. spin relaxation via precession in internal spin-orbit fields) where τ_s scales inversely with τ_p [28, 31]. This behavior has been observed in four BLG devices (mobility: 400-1300 cm^2/Vs). Figures 3d and 3e show the temperature dependences of τ_s and D, respectively. At low temperatures, τ_s is enhanced while D is reduced, which is different from SLG where both D and τ_s increase as temperature decreases for most gate voltages. The opposite trends of the temperature dependences of τ_s and D suggest the strong contributions of spin relaxation mechanisms of the DP type, which is also suggested in ref. 32.

To investigate the spin relaxation in BLG quantitatively, we perform a detailed measurement of the gate voltage dependence of a BLG spin valve (device C) at 4 K. In figure 4a, τ_s and D exhibit opposite dependences as a function of gate voltage, indicating the importance of DP spin relaxation. Quantitatively, it is known that the scattering rate for EY spin relaxation scales as $\frac{1}{\tau_s^{EY}} \sim \frac{1}{\tau_p} \sim \frac{1}{D}$, while the scaling for DP spin relaxation is $\frac{1}{\tau_s^{DP}} \sim \tau_p \sim D$ [7, 15, 25-28, 31]. Hence, if both EY and DP spin scattering are present, the spin lifetime is:

$$\frac{1}{\tau_s} = \frac{1}{\tau_s^{EY}} + \frac{1}{\tau_s^{DP}} = \frac{K_{EY}}{D} + K_{DP} D \qquad (2)$$

Figure 4b shows the spin relaxation rate ($1/\tau_s$) as a function of D for BLG (device C at 4 K). The best fit by equation 2 yields $K_{EY} = 0.05 \pm 0.01$ (10^{-2} m^2s^{-1}) ns^{-1}, and $K_{DP} = 1.24 \pm 0.09$ (10^{-2} m^2s^{-1})$^{-1}$ ns^{-1} The contributions from EY spin relaxation are shown by the blue dashed line, and the contributions from DP spin relaxation are shown by the red dashed line. For the experimental range of D, the DP contribution to spin relaxation is much stronger than the EY contribution. For comparison, we plot the spin relaxation rate ($1/\tau_s$) as a function of D (figure 4b inset) for SLG

`

(device A at 4 K). The best fit parameters are K_{EY} = 3.05 ± 0.35 (10^{-2} m^2s^{-1})ns^{-1}, and K_{DP} = -0.02 ± 0.10 (10^{-2} m^2s^{-1})$^{-1}ns^{-1}$, which is zero within the error bars.

It is noted that longer spin lifetimes are observed in BLG (up to 6.2 ns) than in SLG (up to 1.0 ns). Theoretically, the intrinsic spin-orbit coupling in BLG is an order of magnitude larger than in SLG, which predicts shorter spin lifetimes for BLG [30]. The opposite experimental trend verifies that the spin relaxation in graphene is of extrinsic origin and the SLG is more sensitive to the extrinsic spin scattering than BLG. Possible sources of extrinsic EY spin relaxation include long-range (Coulomb) impurity scattering and short-range impurity scattering [13], while an extrinsic DP spin relaxation could arise from curvature of the graphene film [1, 5]. The transition from EY-dominated SLG to the DP-dominated BLG could be due to a strong reduction of the EY contribution because of enhanced screening of the impurity potential in thicker graphene [15, 33] and the smaller surface-to-volume ratio. However, a quantitative explanation for the substantial differences in spin relaxation between SLG and BLG will require further theoretical and experimental studies. Specifically, understanding the relationship between spin relaxation and the characteristics that differentiate SLG from BLG (e.g. band structure, lattice symmetry, bandgap formation in BLG, etc.) may be essential. For example, it has been shown by Dugaev et al. that in the presence of random spin-orbit interactions (which could be produced by curvature domains), the DP-like contribution to the spin lifetime has different values and decreases more rapidly with carrier concentration for massive fermions (BLG case) than for massless fermions (SLG case) [34, 35], even with the same spin-orbit coupling strength. Thus, K_{EY} and K_{DP} should be treated as empirical fitting parameters to quantify the data.

In summary, spin relaxation in SLG and BLG spin valves has been investigated. By studying the spin lifetime and diffusion coefficient in SLG and BLG as a function of temperature and

`

carrier concentration, contrasting behaviors are observed. For SLG, the EY spin scattering (e.g. impurity scattering) is dominant at low temperatures leading to the linear scaling of τ_s and τ_p. For BLG, the temperature dependence shows an opposite trend between the spin lifetime and momentum scattering time, and the low temperature gate voltage dependence shows an inverse relationship of the two quantities, which indicate the dominance of DP spin relaxation.

We acknowledge technical assistance and discussion with E. Sherman, K. M. McCreary, H. Wen, J. J. I. Wong, A. G. Swartz, K. Pi and Y. Li and the support of ONR (N00014-09-1-0117), NSF (DMR-1007057), and NSF (MRSEC DMR-0820414).

References:

[1] D. Huertas-Hernando, F. Guinea, and A. Brataas, Phys. Rev. B **74**, 155426 (2006).
[2] H. Min *et al.*, Phys. Rev. B **74**, 165310 (2006).
[3] Y. Yao *et al.*, Phys. Rev. B **75**, 041401(R) (2007).
[4] B. Trauzettel *et al.*, Nature Physics **3**, 192 (2007).
[5] D. Huertas-Hernando, F. Guinea, and A. Brataas, Phys. Rev. Lett. **103**, 146801 (2009).
[6] N. Tombros *et al.*, Nature **448**, 571 (2007).
[7] C. Józsa *et al.*, Phys. Rev. B **80**, 241403(R) (2009).
[8] M. Popinciuc *et al.*, Phys. Rev. B **80**, 214427 (2009).
[9] M. Shiraishi *et al.*, Adv. Funct. Mater. **19**, 3711 (2009).
[10] W. Han *et al.*, Appl. Phys. Lett. **94**, 222109 (2009).
[11] K. Pi *et al.*, Phys. Rev. Lett. **104**, 187201 (2010).
[12] W. Han *et al.*, Phys. Rev. Lett. **105**, 167202 (2010).
[13] A. H. Castro Neto, and F. Guinea, Phys. Rev. Lett. **103**, 026804 (2009).
[14] C. Ertler *et al.*, Phys. Rev. B **80**, 041405(R) (2009).
[15] T. Maassen *et al.*, arXiv:1012.0526 (2010).
[16] K. S. Novoselov *et al.*, Science **306**, 666 (2004).
[17] A. C. Ferrari *et al.*, Phys. Rev. Lett. **97**, 187401 (2006).
[18] See supplementary material for detailed descriptions.
[19] M. Johnson, and R. H. Silsbee, Phys. Rev. Lett. **55**, 1790 (1985).
[20] F. J. Jedema *et al.*, Nature **416**, 713 (2002).
[21] X. Lou *et al.*, Nature Physics **3**, 197 (2007).
[22] S. Cho, Y.-F. Chen, and M. S. Fuhrer, Appl. Phys. Lett. **91**, 123105 (2007).
[23] W. Han *et al.*, Phys. Rev. Lett. **102**, 137205 (2009).
[24] H. Goto *et al.*, Appl. Phys. Lett. **92**, 212110 (2008).
[25] J. Fabian *et al.*, Acta Physica Slovaca **57**, 565 (2007).
[26] R. J. Elliott, Phys. Review **96**, 266 (1954).

`

[27] Y. Yafet, in Solid State Physics, edited by F. Seitz and D. Turnbull (Academic Press Inc., New York, 1963), Vol. 14, p. 1.
[28] F. Meier, and B. P. Zachachrenya, Optical Orientation, Modern Problems in Condensed Matter Science (North-Holland, Amsterdam, 1984), Vol. 8.
[29] A. K. Geim, and K. S. Novoselov, Nature Materials **6**, 183 (2007).
[30] F. Guinea, New J. of Phys. **12**, 083063 (2010).
[31] M. I. D'yakonov, and V. I. Perel', Sov. Phys. State **13**, 3023 (1972).
[32] T.-Y. Yang *et al.*, arXiv:1012.1156 (2010).
[33] F. Guinea, Phys. Rev. B **75**, 235433 (2007).
[34] V. K. Dugaev *et al.*, Phys. Rev. B 80, 081301(R) (2009).
[35] V. K. Dugaev, E. Y. Sherman, and J. Barnas, Phys. Rev. B **83**, 085306 (2011).

Figure Captions:

Fig. 1. (a) Nonlocal MR measurement of device A (SLG) at 300 K. The red (black) curve is measured as the field is swept up (down). E1 and E4 are Au electrodes (labeled 1 and 2), and E2 and E3 are Co electrodes (labeled 2 and 3). The large change in R_{NL} indicated by the red arrow is due to the injection and transport of spin from E2 to E3. (b) Hanle measurements of device A at 300 K. The red (black) circles are data taken for parallel (antiparallel) Co magnetizations. The solid lines are the best fit by equation 1. (c-d) Spin lifetime (squares) and diffusion coefficient (circles) as a function of gate voltage at 300 K and 4 K respectively.

Fig. 2. Temperature dependence of SLG spin valves (device A). (a-b) Temperature dependence of spin lifetime and diffusion coefficient at different gate voltages relative to the charge neutrality point. (c-f) Plot of spin lifetime vs. diffusion coefficient at T = 4 K, T = 10 K, T = 50 K and 100 K, T = 200 K and 300 K, respectively. The dotted line is a linear fit of the spin lifetime vs. diffusion coefficient.

`

Fig. 3. Gate and temperature dependence of BLG spin valves (device B). (a) Hanle measurement at 20 K for $V_g = V_{CNP}$. Inset: Hanle measurement at 300 K for $V_g = V_{CNP}$. (b-c) Spin lifetime (squares) and diffusion coefficient (circles) as a function of gate voltage at 300 K and 20 K. (d-e) Temperature dependence of spin lifetime and diffusion coefficient at different gate voltages relative to the charge neutrality point.

Fig. 4. Gate voltage dependence of BLG spin valves (device C). (a) Spin lifetime (squares) and diffusion coefficient (circles) as a function of gate voltage at 4 K. (b) Spin relaxation rate as a function of diffusion coefficient. The black solid line is the best fit based on equation 2. The dashed red (blue) line is the contribution of DP (EY) spin relaxation. Inset: Spin relaxation rate as a function of diffusion coefficient for SLG (device A) at 4K with the best fit (solid line) based on equation 2.

Figure 1

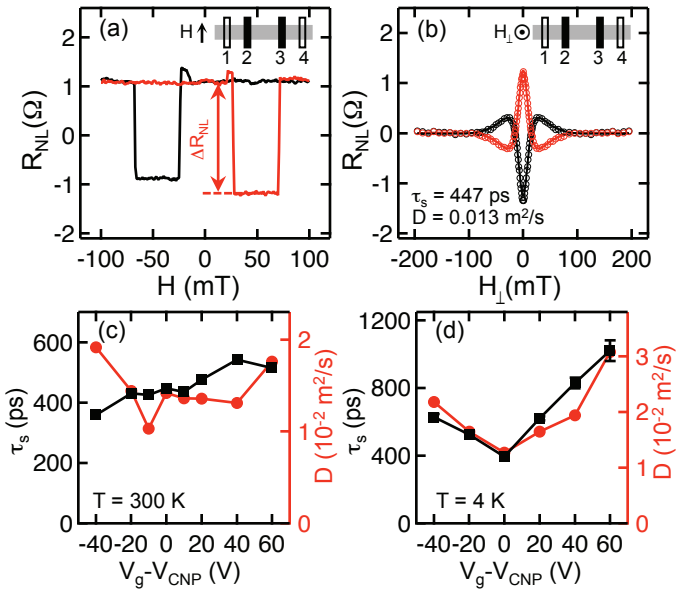
(a)
H
1 2 3 4
ΔR_{NL}
R_{NL} (Ω)
H (mT)
(b)
$H_\perp$
τ_s = 447 ps
D = 0.013 m²/s
$H_\perp$(mT)
(c)
T = 300 K
τ_s (ps)
D (10^{-2} m²/s)
V_g-V_{CNP} (V)
(d)
T = 4 K

Figure 2

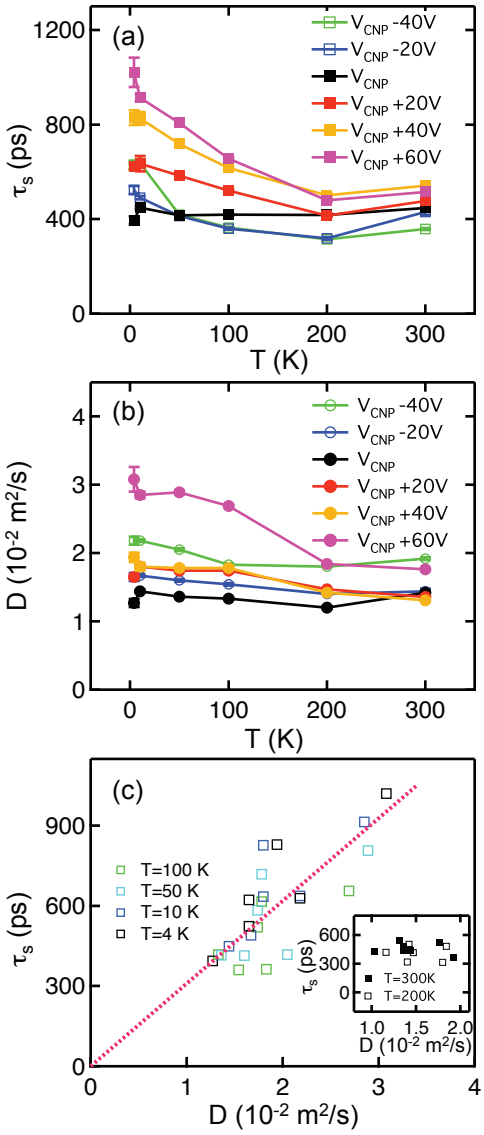
(a)
V_{CNP} -40V
V_{CNP} -20V
V_{CNP}
V_{CNP} +20V
V_{CNP} +40V
V_{CNP} +60V
τ_s (ps)
T (K)
(b)
D (10^{-2} m^2/s)
(c)
T=100 K
T=50 K
T=10 K
T=4 K
T=300K
T=200K
D (10^{-2} m^2/s)

Figure 3

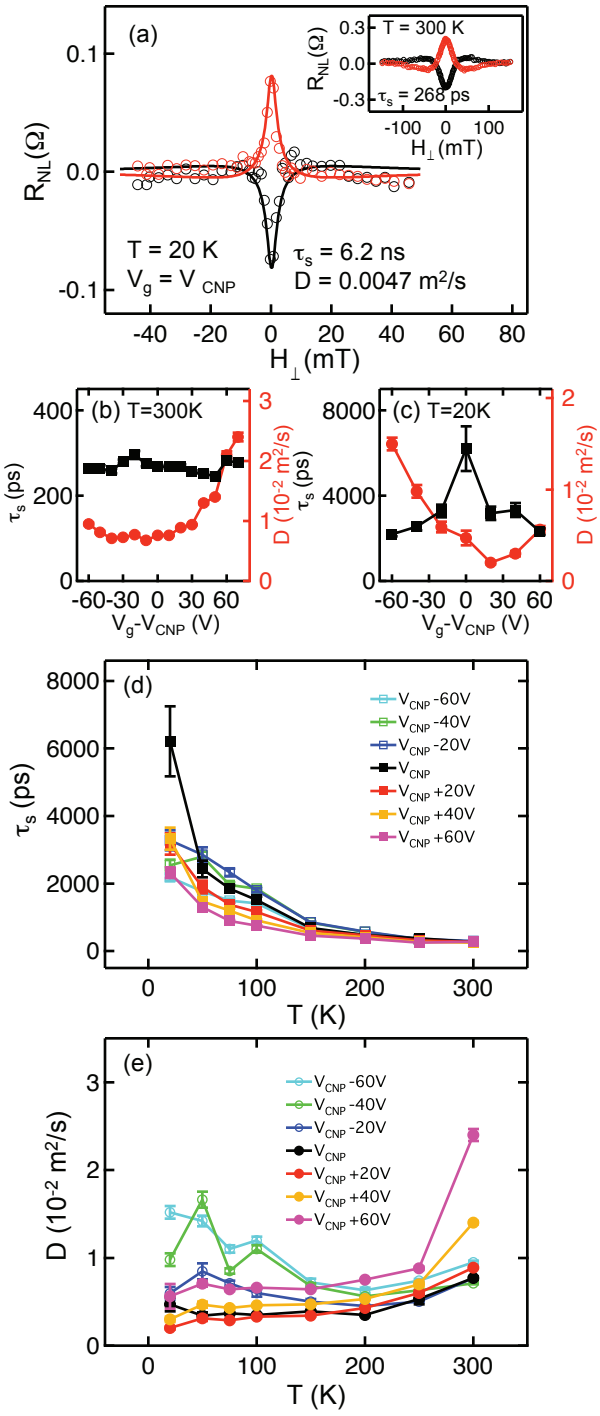
(a)
T = 300 K
τs = 268 ps
RNL (Ω)
H⊥ (mT)
T = 20 K
Vg = V CNP
τs = 6.2 ns
D = 0.0047 m²/s
(b) T=300K
(c) T=20K
τs (ps)
D (10⁻² m²/s)
Vg-VCNP (V)
(d)
(e)
VCNP -60V
VCNP -40V
VCNP -20V
VCNP
VCNP +20V
VCNP +40V
VCNP +60V
T (K)

Figure 4